

Virtual Goniophotometric Measurements Protocol

Aravind Krishnaswamy
School of Computer Science
University of Waterloo

Gladimir V. G. Baranoski
School of Computer Science
University of Waterloo

Jon G. Rokne
Department of Computer Science
University of Calgary

Technical Report CS-2002-21
July, 2002

Abstract

Many scattering models have been proposed in the graphics literature. Few of them, however, have been evaluated through comparisons with real measured data. As the demand for plausible and predictable scattering models increases, more effort is focused on performing such comparisons. In this paper we examine the implementation of virtual goniophotometric devices used to evaluate algorithmic scattering models, focusing on practical issues, namely the subdivision of the collector sphere and the ray density required to obtain reliable BRDF and BTDF estimates. Our discussion of these issues is supported by experiments whose results are also presented in this paper.

1 Introduction

The group of measurements necessary to characterize both the color and surface finish of an object is called the *measurement of appearance* of an object [15]. This group of measurements involves the spectral energy distribution of propagated light, and the spatial energy distribution of that light, measured in terms of *bidirectional surface-scattering distribution function* (BSSDF, or simply BDF). The changes in the spatial distribution of the propagated light affect appearance characteristics such as gloss, reflection haze, transmission haze, luster and translucency.

Actual BDF measurements are performed using goniophotometers [15, 17]. In this paper we discuss computer simulations of these devices, henceforth called virtual goniophotometers. The use of such devices gives us control over the spectral data generation from computer models used to simulate the scattering profile of various materials, and allows us to perform experiments at different sampling resolutions, which are important requirements in rendering. Besides their use in data collection, these devices can also be used to determine the plausibility of scattering models.

When virtual measurement devices are discussed in the computer graphics literature they are usually presented in connection with a scattering model. For example, Gondek *et al.* [11] have used a device for spectral and spatial measurements, a virtual goniospectrophotometer, presented as an optics model and a capture dome used in conjunction with a geometric model of surface microstructure. Although our discussion is related to applications involving algorithmic models, our main goal is to describe the formulation of virtual goniophotometers, and to examine implementation issues (collector sphere subdivision and ray density) that affect the accuracy/cost ratio of the measurements, without focusing on any specific model.

The remainder of this paper is organized as follows. In Section 2, we provide goniophotometric background information. In Section 3, we highlight the main applications associated with this research, and present the general formulation of virtual goniophotometers. In Sections 4 and 5, we discuss issues that affect both the accuracy and efficiency of these virtual devices, namely the subdivision of the collector sphere and the ray density of the measurements. This discussion is supported by experiments described in Section 6. Finally, in Section 7, we summarize the main aspects of this research.

2 Goniophotometric Background

2.1 Spatial Light Distribution

The BDF has two components, namely the *bidirectional reflectance distribution function* (BRDF), f_r , and the *bidirectional transmittance distribution function* (BTDF), f_t . It is usually expressed in terms of the ratio between the spectral radiance propagated at a point x of a surface in the direction ψ and the spectral radiant energy (per unit of area and per unit of time) incident from a direction ψ_i at the point x of the surface:

$$f(x, \psi_i, \psi, \lambda) = \frac{dL(x, \psi, \lambda)}{L_i(x, \psi_i, \lambda) d\vec{\omega}_i \cos\theta_i} = \begin{cases} f_r(x, \psi_i, \psi, \lambda) & \text{if } \theta_i < 90^\circ \\ f_t(x, \psi_i, \psi, \lambda) & \text{if } \theta_i > 90^\circ \end{cases} \quad (1)$$

where:

- $f(x, \psi_i, \psi, \lambda)$ = BDF of the surface at x ,
- $dL(x, \psi, \lambda)$ = spectral radiance propagated at x and in a direction ψ ,
- $L_i(x, \psi_i, \lambda)$ = spectral incident radiance at x and in a direction ψ_i ,
- θ_i = angle between the surface normal at x_i and the direction ψ_i ,
- $d\vec{\omega}_i$ = differential solid angle at which L_i arrives at x .

An important property of the BDF is its symmetry or reciprocity condition, which is based on *Helmholtz Reciprocity Rule*¹ [4]. This rule states that the BDF for a particular point and incoming and outgoing directions remains the same if these directions are exchanged. It allows,

¹The original statement of *Helmholtz Reciprocity Rule* does not include non-specular reflection of any sort [4, 31]. Recently Veach [31] derived a reciprocity condition for general BDFs using Kirchhoff's laws regarding radiative transfer [30].

for instance, the “forward” simulation of light rays traveling from a viewer to a light source, which is used by global illumination methods [18, 26]. Quantitatively, this condition can be expressed as:

$$f(x, \psi_i, \psi, \lambda) = f(x, \psi, \psi_i, \lambda) \quad (2)$$

Another important property of the BDFs is that they must be normalized, *i.e.*, conserve energy. This means that the total energy propagated in response to some irradiation must be no more than the energy received [10]. In other words, for any incoming direction the radiant power propagated over the hemisphere can never be more than the incident radiant power [20]. Any radiant power that is not propagated is absorbed. Formally, in the case of reflection of light, the so-called directional-hemispherical reflectance [1] should therefore be less than or at most equal to 1:

$$\rho(x, \psi_i, 2\pi, \lambda) = \int_{outgoing \ \psi} f_r(x, \psi_i, \psi, \lambda) \cos \theta d\vec{\omega} \leq 1, \quad \forall \psi_i \in \text{incoming directions} \quad (3)$$

where:

$$\begin{aligned} f_r(x, \psi_i, \psi, \lambda) &= \text{BRDF of the surface at } x, \\ \theta &= \text{angle between the surface normal and the outgoing direction } \psi, \\ d\vec{\omega} &= \text{differential solid angle at which the radiance is reflected.} \end{aligned}$$

A similar relation given in terms of the directional-hemispherical transmittance [1] and the BTDF is used for the transmission of light. BRDF and BTDF models, or simply BDF models, that are energy-conserving and reciprocal are considered *physically plausible*². This is a crucial requirement for physically-based rendering frameworks aimed at global illumination applications.

2.2 General Characteristics of Actual Goniophotometers

A goniophotometer (from greek: gonio-photo-meter=angle-light-measuring) is defined as an instrument that measures radiant flux (power) as a function of angles of illumination and observation [7]. These measurements can be performed in different ways, and, as a result, there are many possible configurations for these devices. Computer graphics researchers have proposed extensions for industry made goniophotometers [9] as well as new designs based on the use of digital cameras [19, 32, 24]. A review of these devices is beyond the scope of this work. A reader interested in more detailed description of goniophotometers used in computer graphics is referred to more comprehensive works in this area [9, 25].

Goniophotometers are also important basic tools for fundamental research in colorimetry [23], solar engineering [8], plant biochemistry [3, 16] and remote sensing [6, 16]. For instance, Figure 1 shows photographs of a goniophotometer used by Combes *et al.* [5] to measure BDFs of plant specimens. The light flux which is incident on the specimen comes from an emitter. After being reflected or transmitted by the specimen, it is captured by a detector (photometer). For BRDF measurements the detector(s) are placed in hemisphere above the specimen (Figure 1a) and for BTDF measurements the detector(s) are placed in hemisphere below the specimen (Figure 1b).

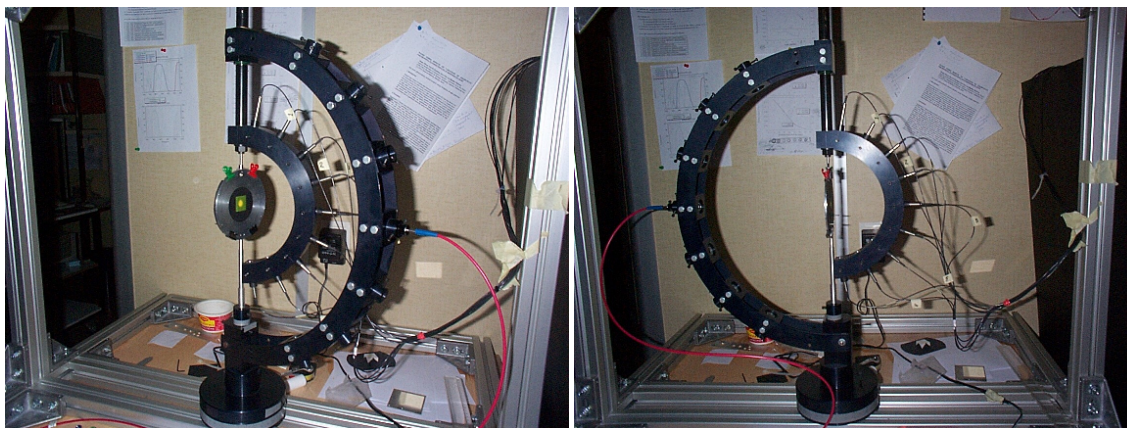


Figure 1: Photographs of a goniophotometer showing different set-ups for: BRDF (left) and BTDF (right) measurements. (Courtesy of Stephane Jacquemoud.)

A comprehensive goniophotometric record for a simple specimen would require a formidable number of measurements as mentioned by Judd and Wyszecki [17] and Greenberg *et al.* [13]. Both the emitter and the photometer would have to be moved independently of one another to every position on the hemisphere. In order to illustrate this aspect Judd and Wyszecki perform the following calculation. Suppose that one works with a fairly large solid angle of approximately 0.005 steradian for each aperture. To cover the entire hemisphere (2π steradian) as closely as possible with such an aperture without overlapping, we must use about 1000 different positions. With both the source and the photometer moved in each of the 1000 positions one ends up making 1 million measurements!

For many specimens the most informative goniophotometric data are taken in the plane containing the direction of the incident light and the normal of the specimen. Many actual goniophotometers are abridged to this extent. The emitter movement goes from $\theta_i = 0^\circ$ to $\theta_i = 90^\circ$

²Lewis [21, 22] uses the term “plausible” to describe BDF models whose existence does not violate the laws of physics.

and the photometer movement ranges $\theta_i = 90^\circ$ to $\theta_r = -90^\circ$. Assuming the same aperture sizes as before, this abridged goniophotometric record would contain $18 \times 36 = 640$ data points.

The best-designed, best-constructed and best-calibrated spectrophotometers still yield results that differ from one measurement to the next. These differences, or uncertainties, are net results of combinations of many small fluctuations due to independent variations of different components of the instrument, different factors in the environment and how the specimen is handled.

3 Virtual Goniophotometry

3.1 Applications

Two applications of virtual measurements are especially relevant for biologically and physically-based rendering. The first application corresponds to virtual measurements aimed at the testing and evaluation of BDF models through comparisons with actual measurements. Obviously, these models can be verified against measurements of real materials. However, in order to obtain the readings from a computer model in the first place, one must perform a computer simulation of the inputs and outputs of the model, *i.e.*, use a virtual goniophotometer. In this case, in order to minimize the introduction of bias in the comparisons, the formulation of this virtual device has to reproduce actual measurement conditions as faithfully as possible.

The second application corresponds to data generation from previously validated computer models. This may involve a large number of measurements with respect to different wavelengths and illuminating geometries. Such data can sometimes be found in the literature where actual measurements from real materials are reported. However, more often it is not available, and, even when it is available, it is only for a restricted number of measurement configurations. The use of virtual goniophotometers allows the removal of this restriction.

3.2 General Formulation of Virtual Goniophotometers

In order to simulate radiance measurements performed by placing the photometer at different viewing positions, one can use radiance detectors, which are represented by the patches of a collector sphere placed around a specimen. Figure 2 presents a sketch showing the principal components of a virtual goniophotometer and their geometrical arrangement. The light flux incident on the specimen comes from the emitter through patch I . The light flux viewed by the photometer is delimited by patch V . Both the direction of illumination and viewing can be varied independently within the hemisphere above the specimen. The position of emitter and patch I is given by its azimuthal angle ϕ_i and its polar angle θ_i . The position of photometer and patch V is given by its azimuthal angle ϕ_r and its polar angle θ_r .

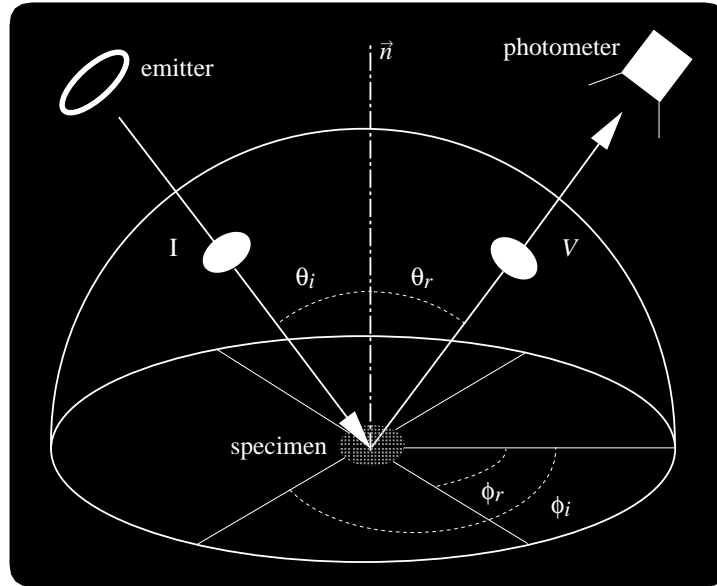


Figure 2: Sketch of a virtual goniophotometer.

Using this arrangement, the BRDF for a direction associated with a given radiance detector placed in the upper hemisphere can be determined in terms of radiant power. More specifically, it is given by the ratio between the radiant power reaching the detector, Φ^r , after interacting with the specimen, and the incident radiant power, Φ^i [12].

The corresponding expression used to compute the BRDF for light incident at wavelength λ , considering the solid angle in the direction of incidence, ω_i , and the solid angle in the direction associated with the radiance detector, ω_r , is given by:

$$f_r(\lambda, \omega_i, \omega_r) = \frac{\Phi^r(\lambda)}{\Phi^i(\lambda) \omega_r^p} \quad (4)$$

where:

ω_r^p = projected solid angle regarding the direction associated with the radiance detector.

In turn, the projected solid angle $\vec{\omega}_r^p$ is given by:

$$\vec{\omega}_r^p = \frac{A_r \cos \theta_r}{L^2} \quad (5)$$

where:

- A_r = area of the radiance detector,
- L = distance from the specimen to the radiance detector,
- θ_r = angle between the direction associated with the radiance detector and the specimen normal.

Consider N rays shot towards the specimen for a given wavelength λ , and assume that each ray carries the same amount of radiant power, Φ . If the total radiant power to be shot is Φ_i , then the radiant power carried by each ray is given by [26]:

$$\Phi_{ray}(\lambda) = \frac{\Phi_i(\lambda)}{N} \quad (6)$$

Also, the radiant power reaching the radiance detector can be written as:

$$\Phi^r(\lambda) = n_r \Phi_{ray}(\lambda) \quad (7)$$

where:

- n_r = number of rays hitting a radiance detector.

Thus, replacing Equation 6 and Equation 7 in Equation 4, the expression to compute the BRDF reduces to:

$$f_r(\lambda, \vec{\omega}_i, \vec{\omega}_r) = \frac{n_r}{N \vec{\omega}_r^p} \quad (8)$$

Similarly the BTDF is calculated assuming the radiance detectors are placed in the lower hemisphere.

For applications involving data generation from a previously validated model, the sample rays are usually collimated, *i.e.*, the sample rays have the same origin and hit the specimen at the same point. For applications involving comparisons with actual measurements the actual measurement conditions must be reproduced as faithfully as possible. In these situations the sample rays are distributed angularly according to the geometrical arrangement of the surfaces used to represent the emitter and the specimen. As mentioned by Crowther [6], the incident radiation from an emitter shows no preference for one angular region over the other. So, in order to simulate these measurement conditions, the origins and targets of the rays are random points (or sample points) chosen on the surfaces used to represent the emitter and the specimen respectively. Several sampling strategies can be used to select these sample points. In this paper we do not intend to determine the most accurate or the most efficient sampling strategy. The merits and drawbacks of different sampling strategies have been adequately covered elsewhere [10, 26, 28].

For the sake of completeness, we indicate a strategy that can be used in these applications, which is based on the classical Monte Carlo stratified sampling [14] or jittered sampling [26]. It uses a warping transformation to guarantee that the sample points are reasonably equidistributed on a disk of radius \mathcal{R} . This transformation is based on the following probability distribution function [27]:

$$\Gamma(x, y) = \frac{1}{\pi \mathcal{R}^2} \quad (9)$$

which enables the computation of the pair (x, y) through the following warping function [29]:

$$(x, y) = \begin{cases} \left(\frac{\pi}{4} \cdot \frac{\xi_2}{\xi_1}, \xi_1 \mathcal{R} \right) & \text{if } \xi_1 > -\xi_2 \text{ and } \xi_1 > \xi_2 \\ \left(\frac{\pi}{4} \cdot \left(2 - \frac{\xi_2}{\xi_1} \right), \xi_2 \mathcal{R} \right) & \text{if } \xi_1 > \xi_2 \text{ and } \xi_1 > -\xi_2 \\ \left(\frac{\pi}{4} \cdot \left(4 - \frac{\xi_2}{\xi_1} \right), -\xi_1 \mathcal{R} \right) & \text{if } \xi_1 < \xi_2 \text{ and } \xi_1 < \xi_2 \\ \left(\frac{\pi}{4} \cdot \left(6 - \frac{\xi_2}{\xi_1} \right), -\xi_2 \mathcal{R} \right) & \text{otherwise} \end{cases} \quad (10)$$

where $\xi_1, \xi_2 \in [-1, 1]$. This warping function preserves fractional area and is bicontinuous, thus if ξ_1 and ξ_2 are randomly equidistributed the function guarantees their points on the disk will also be randomly equidistributed.

After generating the x and y coordinates of a sample point, the z coordinate is added. For a sample point on the specimen, z is equal to zero, and, for a sample point on the emitter, z will correspond to the distance D between the disks. Finally, to obtain the origin of a sample ray, the corresponding sample point (x, y, z) on the emitter shall be rotated according to a specified incidence geometry given by ϕ_i and θ_i .

4 Collector Sphere Subdivision

4.1 Equal Angular Intervals

The simplest way to subdivide the collector sphere into patches is to use spherical coordinates, $\phi \in [0, 2\pi]$ and $\theta \in [0, \frac{\pi}{2}]$ (Figure 3), sampled at equal angular intervals along both coordinate directions. In this case the resulting patches will not have the same area. Note that the computation of the BDFs involves the computation of the projected solid angle (Equation 5) for each patch, which, in turn involves the computation of the area of the patch and the specification of the angle θ_r .

Consider a patch given by the spherical coordinates (θ_1, θ_2) and (ϕ_1, ϕ_2) (Figure 3). Intuitively θ_r should correspond to $\frac{\theta_1 + \theta_2}{2}$. Note that in the computation of the projected solid angle we need to compute the $\cos \theta_r$. Our experiments (Figure 4) show that using $\theta_r = \cos\left(\frac{\arccos(\theta_1) + \arccos(\theta_2)}{2}\right)$, one can obtain more uniform results when the sphere is subdivided into a small number of patches. As one subdivides the sphere into a larger number of patches, the differences decrease, since θ_r tends to be same for both approaches.

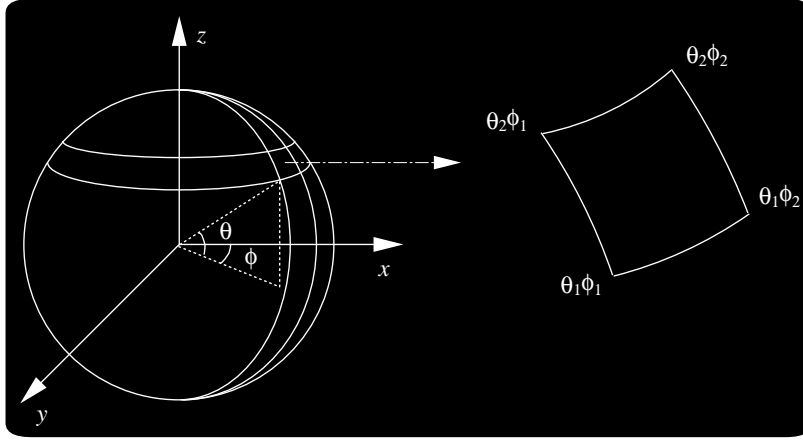


Figure 3: Spherical coordinates used in the subdivision of the collector sphere into patches.

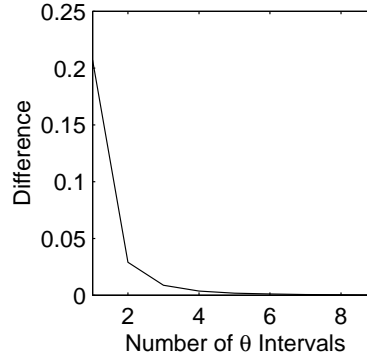


Figure 4: Difference between averaging in terms of $\cos\theta$ and averaging in terms of θ .

4.2 Equal Solid Angles

Another approach that can be applied is the subdivision of the collector sphere into regions of equal solid angles, *i.e.*, the patches on the collector sphere will have the same area. In this case the parameter space represented by $\phi \in [0, 2\pi]$ will be divided into equal intervals as in the previous case. The values for the spherical coordinate θ are chosen to guarantee equal area patches.

Considering the geometry presented in Figure 5, the small triangle has the relationship:

$$\frac{dh}{ds} = \cos\theta \quad (11)$$

and the large the relationship:

$$\frac{h}{L} = \sin\theta \quad (12)$$

and

$$\frac{L'}{L} = \cos\theta \quad (13)$$

so

$$L' = L \cos\theta \quad (14)$$

The integral of the spherical segment between h_1 and h_2 is therefore:

$$\int_{h_1}^{h_2} 2\pi L' ds = \int_{h_1}^{h_2} 2\pi L \cos\theta \frac{dh}{\cos\theta} = \int_{h_1}^{h_2} 2\pi L dh = 2\pi L (h_2 - h_1) \quad (15)$$

Hence, each slice of the same thickness, $(h_2 - h_1)$, has the same surface area around the slice.

Considering the upper hemisphere divided into m_s equal thickness slices, the angles θ_1 and θ_2 limiting a given patch are given by:

$$\theta_1 = \arccos\left(\frac{h_1}{L}\right) \quad (16)$$

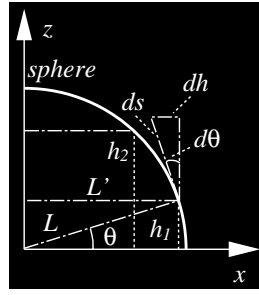


Figure 5: Geometry used to subdivide the collector sphere into equal solid angle regions.

and

$$\theta_2 = \arccos\left(\frac{h_1 + \frac{L}{m_s}}{L}\right) \quad (17)$$

The issues raised in the previous section with respect to the choice for θ_r also apply to this subdivision approach. In fact our experiments (Section 6.1) show minor improvements in the accuracy of the measurements. The computation of the areas, however, can be done more efficiently than in the previous case, since all patches have the same area. In the equal angular intervals technique the areas are not the same for all patches, which results in more flops expended in their computation.

4.3 Equal Projected Solid Angles

The third approach examined in this paper subdivides the collector sphere into regions of equal projected solid angles. Like in the previous cases, the parameter space represented by $\phi \in [0, 2\pi]$ is divided into equal intervals. The values for the spherical coordinate θ are computed taking into account the definition of projected solid angles.

Consider the upper hemisphere above the specimen. Its projected solid angle is given by:

$$\int_{\phi=0}^{\phi=2\pi} \int_{\theta=0}^{\theta=\pi/2} \cos\theta \sin\theta \, d\theta \, d\phi = 2\pi \left[\frac{\cos^2 0}{2} - \frac{\cos^2 \frac{\pi}{2}}{2} \right] = \pi \quad (18)$$

Using the integration above, the projected solid angle of a slice limited by θ_1 and θ_2 is given $\pi[\cos^2\theta_1 - \cos^2\theta_2]$. Considering the hemisphere divided into m_s slices along the parameter space represented by θ , we can obtain the following relationship:

$$\theta_2 = \arccos \sqrt{\cos^2\theta_1 - \frac{1}{m_s}} \quad (19)$$

In this approach the choice of θ_r is embedded in the integration leading to the equal projected solid angles. As a result, the computation of the projected solid angles is performed more accurately and efficiently. Moreover, our experiments (Section 6.1) show that the convergence of the BDF values is uniform even considering a small number of patches, no matter their position.

5 Ray Density

Another key question to be addressed when performing virtual goniophotometric measurements is how many rays should be cast by the emitter element, *i.e.*, how large should N be. Using a sufficiently large number of sample rays, one will have a high probability of obtaining estimates within the region of asymptotic convergence of the expected values of a BDF being measured. The computational costs, however, grow linearly with respect to the total number of sample rays N since the implementation cost is constant per ray. The purpose of the following analysis is, therefore, to determine a satisfactory bound for N such that we can obtain BDF estimates with a higher reliability/cost ratio. In this context the term “satisfactory” means taking into account the uncertainty of the actual goniophotometer whose readings we are comparing the measurements with, and aiming at an error tolerance compatible within rendering requirements.

Baranoski *et al.* [2] have shown that the exponential Chebyshev inequality can be applied to obtain a bound for the number of sample rays required to obtain an asymptotically convergent value for the ratio $\frac{n_r}{N}$ with respect to a single radiance detector r . In this case, it can be shown [2] that:

$$P \left\{ \left| \frac{n_r}{N} - p_r \right| < \epsilon \right\} \geq 1 - 2e^{-2N\epsilon^2} \quad (20)$$

where:

- $P(w)$ = probability of w ,
- p_r = probability of a ray hitting the radiance detector r ,
- ϵ = error tolerance.

Theoretically the confidence δ in a estimation is a positive number such that:

$$\delta \geq 1 - P \left\{ \left| \frac{n_r}{N} - p_r \right| < \epsilon \right\} \quad (21)$$

where

$$\delta \geq \frac{1}{4N\epsilon^2} \quad (22)$$

Using the inequalities above, Baranoski *et al.* [2] showed that the bound on the number of sample rays is given by:

$$N = \left\lceil \frac{\ln(\frac{2}{\delta})}{2\epsilon^2} \right\rceil \quad (23)$$

These inequalities can be generalized for m patches (or radiance detectors) as follows:

$$P \left\{ \cap \left(\left| \frac{n_i}{N} - p_i \right| < \epsilon \right) \right\} = \prod_{i=1}^m P \left\{ \left| \frac{n_i}{N} - p_i \right| < \epsilon \right\} \leq \prod_{i=1}^m (1 - 2e^{-2N\epsilon^2}) \leq 1 - \left(\sum_{i=1}^m 2e^{-2N\epsilon^2} \right) = 1 - 2m e^{-2N\epsilon^2} \geq 1 - \delta^m \quad (24)$$

Resulting in:

$$\delta \geq \sqrt[m]{2m} e^{-\frac{2N\epsilon^2}{m}} \quad (25)$$

For large values of m , the inequality above reduces to:

$$\delta \geq e^{-\frac{2N\epsilon^2}{m}} \quad (26)$$

and the number of rays is given by:

$$N = m \left\lceil \frac{\ln(\frac{2}{\delta})}{2\epsilon^2} \right\rceil \quad (27)$$

6 Experimental Evaluation

The experiments presented in this section address implementation and usage issues directly associated with the reliability of virtual goniophotometers in general, *i.e.*, we are not targeting the reproduction of measurements performed by a specific goniophotometer. Hence, we use a virtual device whose collector sphere has unit radius and consider collimated incident beams in these experiments. For the sake of consistency we use the same angle of incidence (45°) in all experiments. Since the procedures are the same for both BRDF and BTDF measurements, we focus our observations in the former and work with the upper hemisphere.

6.1 Subdivision Errors

In our evaluation of error propagation associated with subdivision techniques described in Section 4 (Figure 6), we consider a specimen with perfect diffuse (Lambertian) reflective properties for two reasons. First, its BRDF with respect to any direction is known, *i.e.*, $f_r = \frac{1}{\pi} = 0.3183$, which is convenient for error comparisons. Second the cosine distributions of the reflected rays allow a better comparison of the error propagation with respect to different collector patches. In our experiments we use a collector hemisphere with a resolution of 30×30 patches giving 900 outgoing directions, which would be enough to allow comparisons with a typical set of actual measurements for a single isotropic material [13].

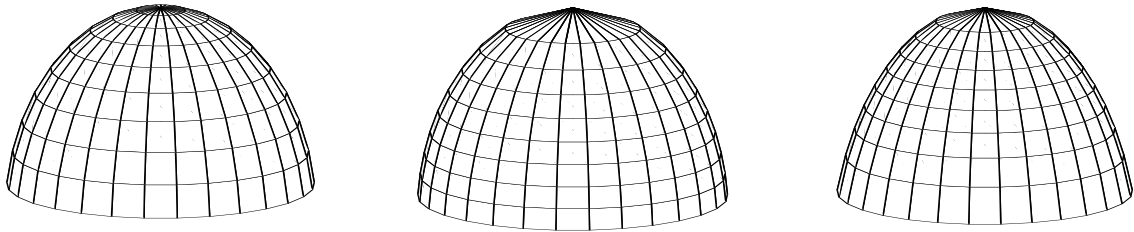


Figure 6: Subdivision techniques: equal angular intervals (left), equal solid angles (middle), equal projected solid angles (right).

Figure 7 presents root-mean-square (RMS) error[10] comparisons considering the three subdivisions described earlier. Although the RMS error is lower for experiments using the equal projected solid angle strategy, the differences decrease with an increase in the number of rays as expected.

It is worth noting, however, that the RMS is a global measure, *i.e.*, low RMS error does not guarantee low error for individual patches. The graphs presented in Figure 8 show the BRDF values for three patches on a same plane (fixed ϕ), top, middle and bottom (grazing angle). As we can see, using the the equal projected solid angle strategy (Figure 8c), the BRDF values with respect to three patches converge more uniformly to the actual value than using the other techniques (Figure 8a and 8b).

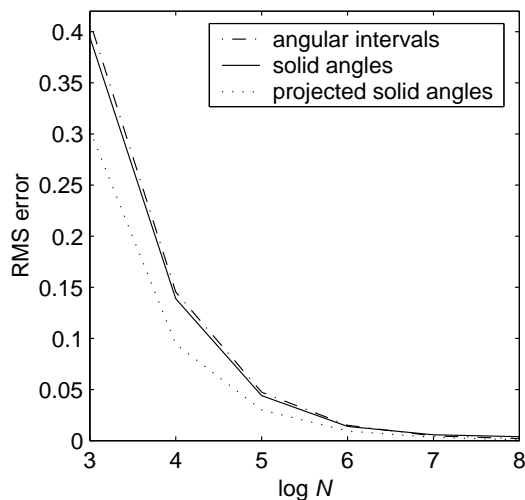


Figure 7: RMS error comparisons with respect to BRDF computation (collector hemisphere resolution: 30×30 patches) using the three subdivision techniques examined in this paper.

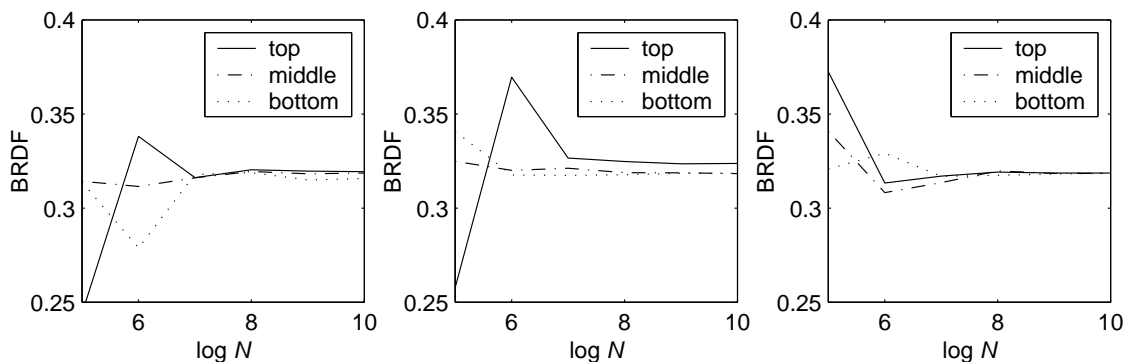


Figure 8: BRDF values for three different patches (collector hemisphere resolution 30×30 patches) using: equal angular intervals (left), equal solid angles (center) and equal projected solid angles (right).

6.2 Ray Density Bound

For virtual goniophotometric measurements aimed at rendering applications one needs solutions accurate to only 1-10%, since humans do not perceive finer variations of light, which, in turn, allow us to set $\delta = 0.1$. Also, according to data provided in the measurement literature [9] the uncertainty of actual goniophotometers is around 0.5% or higher, which allow us to set $\epsilon = 0.005$. Using the proposed upper bound presented in Section 5, the number of rays required to obtain asymptotically convergent readings is given by $N = m10^{5.02}$, where m is total number of patches of the collector hemisphere. In all experiments presented in this section we apply the equal projected solid angles strategy to subdivide the collector hemisphere.

We performed BRDF measurements for a diffuse material using three different resolutions for the collector hemisphere, namely 10×10 , 30×30 and 100×100 patches. Applying the proposed bound for the 10×10 resolution, one can expect asymptotically convergent readings using at most 10^7 rays. For the 30×30 resolution 10^8 rays are sufficient to obtain asymptotically convergent readings, while for the 100×100 resolution one would need a larger number of rays. These aspects can be visually observed in Figure 9 which presents the profiles of these BRDF measurements. These error propagation trends can also be quantitatively verified through the RMS errors presented in Table 1.

Since a computer model is less predictable than measuring physical phenomena, it would be important to verify that the convergence of the measurements is not restricted to a single plane. Figure 10 presents BRDF measurements for the same diffuse material to illustrate this aspect. Furthermore, it is worth noting that this trend is not restricted to Lambertian models as illustrated in Figure 11, which presents BRDF measurements with respect to a model for glossy materials. In fact a Lambertian model was used in these experiments because it represents the worst case scenario in which the rays are evenly distributed among the patches.

For models simulating materials with a stronger specular behavior the number of rays required to obtain asymptotically convergent results will at least one order of magnitude smaller than the number provided by the proposed bound as illustrated in Figure 12. This aspect suggests that m in the proposed bound could be replaced by m' representing the number of patches on the collector sphere within the specular lobe. This parameter, however, is usually unknown *a priori*. If we had an estimate for it, we could also use this estimate to guide a non-uniform distribution of the collector patches. In the extreme case of a mirror-like BRDF, m' is equal to one. Applying the proposed bound $N = 10^{5.05}$ rays would be sufficient to obtain asymptotically convergent results, which corresponds to the number of rays required to obtain

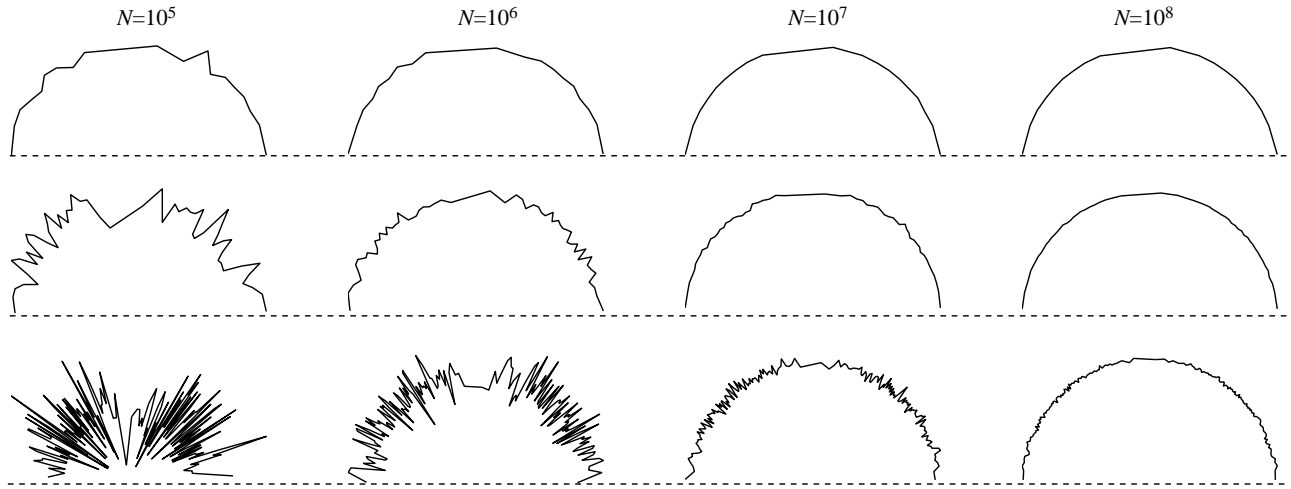


Figure 9: Profiles of BRDF measurements for a diffuse material taken on the plane given by the direction of the incident beam and the normal of the specimen, and using different resolution for the collector hemisphere: 10x10 patches (top), 30x30 patches (middle) and 100x100 patches (bottom).

number of rays	10^5	10^6	10^7	10^8
10x10 patches	0.0091	0.0036	0.0009	0.0003
30x30 patches	0.0301	0.0095	0.0030	0.0009
100x100 patches	0.0995	0.0318	0.0101	0.0033

Table 1: RMS errors associated to BRDF measurements for a diffuse material considering three resolutions for the collector sphere and using four ray densities.

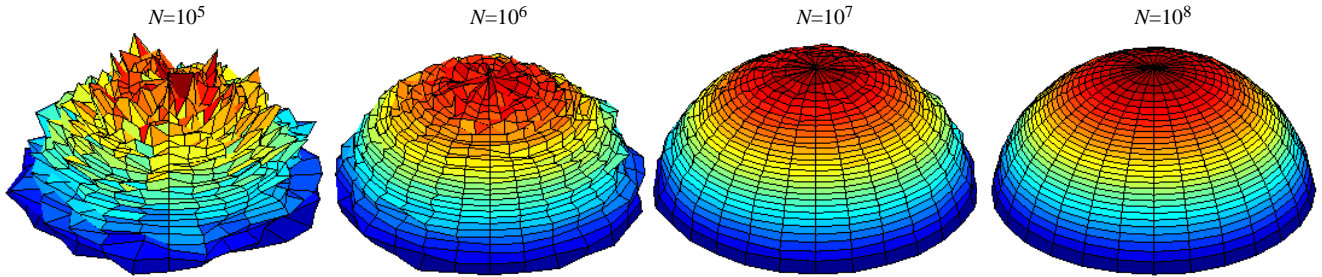


Figure 10: BRDF measurements for a diffuse material obtained using a collector hemisphere subdivided into 30x30 patches and four different ray densities.

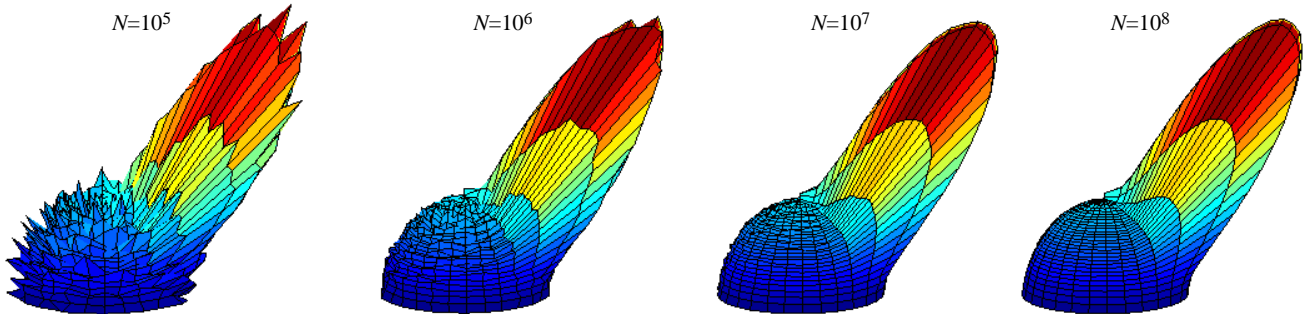


Figure 11: BRDF measurements for a glossy material obtained using a collector hemisphere subdivided into 30x30 patches and four different ray densities.

an asymptotically convergent value for the ratio $\frac{n_r}{N}$ with respect to a single radiance detector (patch).

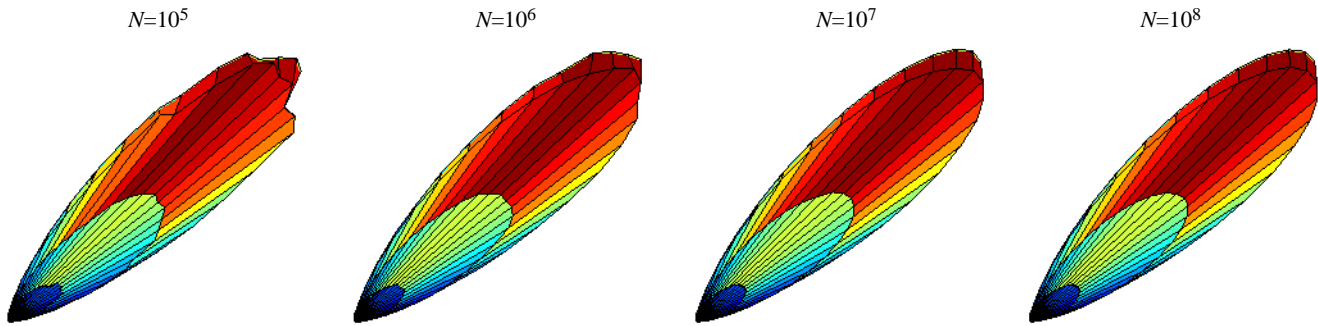


Figure 12: BRDF measurements for a glossy material with a strong specular behavior obtained using a collector sphere subdivided into 30x30 patches and four different ray densities.

7 Conclusion

In this paper we examined practical issues related to the validation of algorithmic scattering models through comparisons of virtual measurements with actual measurements. Considering that many readings are required to obtain a comprehensive goniophotometric record for a single specimen, our discussion was focused in strategies to raise the reliability/cost ratio of these readings. Our experiments suggest that the use of a subdivision technique based on equal project solid angles may provide a more uniform convergence for the BRDF estimates. They also indicate that the proposed upper bound for the number of rays required to obtain asymptotically convergent estimates can be used to reduce the computational costs of the simulations.

References

- [1] ANSI. Nomenclature and definitions for illuminating engineering. In *ANSI/IES RP-6-1986*. Illuminating Engineering Society of North America, New York, 1986.
- [2] G.V.G. Baranowski, J.G. Rokne, and G. Xu. Virtual spectrophotometric measurements for biologically and physically-based rendering. *The Visual Computer*, 17(8):506–518, 2001.
- [3] J. Bonner and J.E. Varner. *Plant Biochemistry*. Academic Press, New York, 1965.
- [4] F.J.J. Clarke and D.J. Parry. Helmholtz reciprocity: Its validity and application to reflectometry. *Lighting Research and Technology*, 17(1):1–11, 1985.
- [5] D. Combes, I. Moya, J. Andlauer, S. Jacquemoud, S. Sinoquet, and C. Varlet-Grancher. Un nouveau dispositif de mesure des propriétés optiques et bidirectionnelles de surface végétales. In *8th International Symposium of Physical Measurements & Signatures in Remote Sensing*, pages 283–284, Aussois, France, 2001. CNES.
- [6] B.G. Crowther. Computer modeling of integrating spheres. *Applied Optics*, 35(30):5880–5886, 1996.
- [7] ASTM Standard E284-91C. Standard terminology of appearance. In L.B. Wolff, S.A. Shafer, and G.E. Healey, editors, *Physics-Based Vision Principles and Practice: Radiometry*, pages 146–161, Boston, 1992. Jones and Bartlett Publishers.
- [8] J. Fendley. An analysis of the measuring procedure for the integrating sphere spectrophotometer. *Solar Energy*, 35(3):281–282, 1985.
- [9] S.C. Foo. A gonio-reflectometer for measuring the bidirectional reflectance of material for use in illumination computation. Master’s thesis, Cornell University, August 1997.
- [10] A.S. Glassner. *Principles of Digital Image Synthesis*. Morgan Kaufmann, San Francisco, 1995.
- [11] J.S. Gondek, G.W. Meyer, and J.G. Newman. Wavelength dependent reflectance functions. In Andrew Glassner, editor, *Proceedings of SIGGRAPH*, pages 213–220, July 1994.
- [12] Y.M. Govaerts. *A model of light scattering in three-dimensional plant canopies: a Monte Carlo ray tracing approach*. PhD thesis, Département de Physique, Faculté des Sciences, Université Catholique de Louvain-la-Neuve, 1995.
- [13] D.P. Greenberg, J. Arvo, E. Lafortune, K.E. Torrance, J.A. Ferwerda, B. Walter, B. Trumbore, P. Shirley, S. Pattanaik, and S. Foo. A framework for realistic image synthesis. In *SIGGRAPH Proceedings, Annual Conference Series*, pages 477–494, 1997.
- [14] J.M. Hammerley and D.C. Handscomb. *Monte Carlo Methods*. Wiley, New York, 1964.
- [15] R.S. Hunter and R.W. Harold. *The Measurement of Appearance*. John Wiley & Sons, New York, second edition, 1987.
- [16] S. Jacquemoud and S.L. Ustin. Leaf optical properties: A state of the art. In *8th International Symposium of Physical Measurements & Signatures in Remote Sensing*, pages 223–332, Aussois, France, 2001. CNES.
- [17] D.B. Judd and G. Wyszecki. *Color in Business, Science and Industry*. John Wiley & Sons, New York, third edition, 1975.
- [18] J. Kajiya. The rendering equation. *Computer Graphics (SIGGRAPH Proceedings)*, 20(4):143–150, August 1986.
- [19] K.F. Karner, H. Mayer, and M. Gervautz. An image based measurement system for anisotropic reflection. *Computer Graphics Forum (EUROGRAPHICS Proceedings)*, 15(3):119–128, August 1996.
- [20] E. Lafortune. *Mathematical Models and Monte Carlo Algorithms for Physically Based Rendering*. PhD thesis, Department of Computer Science, Faculty of Engineering, Katholieke Universiteit Leuven, 1996.
- [21] R.R. Lewis. Making shaders more physically plausible. In M. Cohen and C. Puech, editors, *Proceedings of the Fourth Eurographics Rendering Workshop*, pages 47–62, Paris, June 1993.
- [22] R.R. Lewis. Making shaders more physically plausible. *Computer Graphics Forum*, 13:109–120, June 1994.
- [23] D.L. MacAdam. *Color Measurements Theme and Variations*. Springer Verlag, Berlin, 1981.
- [24] S.R. Marschner. *Inverse Rendering for Computer Graphics*. PhD thesis, Cornell University, 1998.
- [25] S.R. Marschner, E.O.F. Lafortune, S.H. Westin, Kenneth E. Torrance, and D.P. Greenberg. Image-based brdf measurement. Technical Report PCG-99-1, Program of Computer Graphics, Cornell University, January 1999.

- [26] P. Shirley. *Physically based lighting for computer graphics*. PhD thesis, Dept. of Computer Science, University of Illinois, November 1990.
- [27] P. Shirley. Nonuniform random points via warping. In D. Kirk, editor, *Graphics Gems III*, pages 80–83. Academic Press, 1992.
- [28] P. Shirley. *Realistic Ray Tracing*. AK Peters Ltd., 2001.
- [29] P. Shirley and K. Chiu. A low distortion map between disk and square. *Journal of Graphical Tools*, 2(3):45–52, 1997.
- [30] R. Siegel and J.R. Howell. *Thermal Radiation Heat Transfer*. MacGraw-Hill Kogakusha, Tokyo, 1972.
- [31] E. Veach. *Robust Monte Carlo Methods for Light Transport Simulation*. PhD thesis, Stanford University, December 1997.
- [32] G.J. Ward. Measuring and modeling anisotropic reflection. *Computer Graphics (SIGGRAPH Proceedings)*, pages 265–272, July 1992.